Chemistry & Biology, Vol. 12, 181–189, February, 2005, ©2005 Elsevier Ltd All rights reserved. DOI 10.1016/j.chembiol.2004.11.014

Structural Basis for the Highly Selective Inhibition of MMP-13

Christian K. Engel, Bernard Pirard, Sandra Schimanski, Reinhard Kirsch, Jörg Habermann, Otmar Klingler, Volkhard Schlotte, Klaus Ulrich Weithmann, and K. Ulrich Wendt*
Aventis Pharma Deutschland GmbH
A Company of the Sanofi-Aventis Group
Industrial Park Hoechst
D-65926 Frankfurt
Germany

Summary

Inhibitors for matrix metalloproteinases (MMPs) are under investigation for the treatment of cancer, arthritis, and cardiovascular disease. Here, we report a class of highly selective MMP-13 inhibitors (pyrimidine dicarboxamides) that exhibit no detectable activity against other MMPs. The high-resolution X-ray structures of three molecules of this series bound to MMP-13 reveal a novel binding mode characterized by the absence of interactions between the inhibitors and the catalytic zinc. The inhibitors bind in the S1′ pocket and extend into an additional S1′ side pocket, which is unique to MMP-13. We analyze the determinants for selectivity and describe the rational design of improved compounds with low nanomolar affinity.

Introduction

Matrix metalloproteinases (MMPs) are a family of zinc endopeptidases that degrade proteins of the extracellular matrix, including collagens, elastins, matrix glycoproteins, and proteoclycans [1, 2]. Zymogen activation and endogenous tissue inhibitors of matrix metalloproteinases (TIMPs) control MMP activity during normal morphogenesis and tissue homeostasis. Abnormal expression or activity of MMPs has been associated with pathological processes related to metastasis, angiogenesis, and cardiovascular disease, as well as rheumathoid arthritis and osteoarthritis [3].

The approximately 27 currently known human MMPs can be grouped into subfamilies based on their substrate specificity [4, 5]. Enzymes of the collagenase family (MMP-1, -8, and -13) cleave fibrillar collagens at neutral pH. MMP-13 cleaves type II collagen more rapidly than MMP-1 or MMP-8 [6]. Along with enhanced MMP-13 mRNA levels in osteoarthritic joints and breast carcinomas, this provides the rationale for MMP-13 as an attractive target for the treatment of degenerative joint disease and breast cancer [4, 7–9].

Clinical administration of broad-spectrum MMP inhibitors, e.g., marimastat, has disclosed severe adverse effects, such as musculoskeletal pain and tendonitis [10]. Consequently, research has been focused on selective inhibition of those MMPs implicated in the targeted disease pathology [11, 12]. While a number of compounds have been identified that exhibit preferential inhibition of certain MMPs, exclusive inhibition of a single MMP has been much more difficult to achieve [5, 13].

At present, the affinity of most known MMP inhibitors relies on two dominant molecular features: (1) a chelating moiety that interacts with the catalytic zinc ion (e.g., hydroxamate groups) and (2) hydrophobic extensions protruding from the catalytic site into the large and hydrophobic S1′ pocket (P1′ group) [14]. Since the structural differences between MMP family members occur mainly in the S1′ subsite, modifications of the P1′ group have been utilized to introduce inhibitor specificity [5, 15]. In particular, the nature of amino acid 218 (MMP-13 numbering) and the so-called specificity loop (amino acids 244–255), which surrounds the zinc-distal part of the S1′ pocket, are discussed as determinants of specificity [16–18].

Among the known zinc-chelating moieties, the hydroxamate group has often been selected as the functionality of choice [19], but has been correlated to unfavorable pharmacokinetics [20] and may be related to chronic toxicity resulting from metabolic activation of the hydroxamate function. These findings have led to the search for alternate zinc binding groups [19, 21–23]. Recently, Chen et al. [15] have described micromolar inhibitors that occupy the S1′ pocket of MMP-13 without interacting with the catalytic zinc. However, optimizing these inhibitors to low nanomolar affinities required the introduction of a zinc binding moiety and yielded a selectivity of >5800-, 56-, and >500-fold against MMP1, MMP9, and TACE [15].

Here, we report on pyrimidine dicarboxamides, a class of highly selective MMP-13 inhibitors exemplified by compound **1** (Figure 1). The crystal structure of **1** bound to the catalytic domain of MMP-13 reveals a binding mode that is characterized by the absence of interactions between **1** and the catalytic zinc. A related pharmacophore model has been suggested [24].

Based on our crystal structure, the selectivity of **1** is investigated by comparison with known MMP structures, and the unusual binding mode of **1** is exploited to design selective non-zinc-chelating inhibitors with low nanomolar activity.

Results and Discussion

Activity Assays

Pyrimidine dicarboxamide **1** exhibited good activity against MMP-13 (IC_{50} = 6.6 μM) and no detectable inhibition of any other tested enzyme (MMP-1, -2, -3, -7, -8, -9, -10, -12, -14, -16; detection limit at 100 μM). In addition, **1** exhibits good water solubility (500 μM at pH 7.5) and a reasonable oral bioavailability in rats (50%). These properties made the pyrimidine dicarboxamide **1** a promising candidate for further optimization.

Crystal Structures

The crystal structure of **1** in complex with the catalytic domain of MMP-13 (MMP-13cd) was determined to investigate the relationship between the molecular structure of **1** and its high selectivity. Crystals were prepared

*Correspondence: ulrich.wendt@sanofi-aventis.com

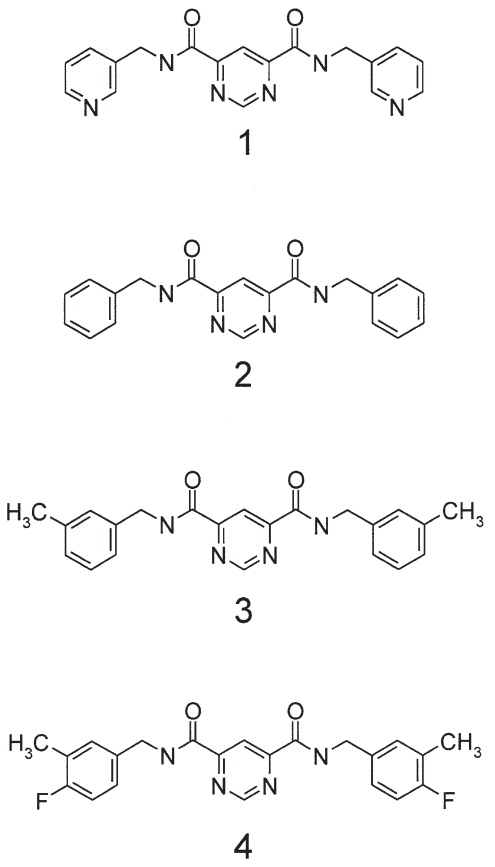

Figure 1. Pyrimidine Dicarboxamide Inhibitors of MMP-13

1, IC_{50} = 6600 nM; **2**, IC_{50} = 400 nM; **3**, IC_{50} = 72 nM; **4**, IC_{50} = 8 nM.

according to the protocol of Lovejoy et al. [16]. Crystallographic results are summarized in Table 1.

The 1.85 Å cocrystal structure of **1** reveals a binding mode that has not been observed for other MMP inhibitors. It is characterized by the absence of interactions between the inhibitor and the catalytic zinc (Figure 2A). The inhibitor binds deeply in the S1′ pocket of MMP-13 from which it protrudes into a side pocket of S1′ that has not been described for other MMPs and is referred to as the S1′* pocket (Figure 2B). The pyridyl substitution closer to the active site (proximal arm) points toward the entrance of the S1′ pocket and does not approach the catalytic zinc closer than 5.5 Å. The pyridyl substitution pointing away from the catalytic zinc (distal arm) protrudes from the S1′ pocket into the adjacent S1′* pocket. Overall, **1** exhibits a bent conformation in which the central pyrimidine dicarboxamide scaffold is tightly packed onto the side chain of Leu218, while the two pyridyl substitutions are embracing the Leu218 side chain like gripping pliers (Figure 3A). The oxo groups of the central scaffold form hydrogen bonds with the main chain of Thr245 and Thr247 and the side chain of Thr247 in the specificity loop (Figures 3A and 3B). The nitrogens of both pyridyl rings form hydrogen bonds with well-defined water molecules (Figure 3A). Of these, the water at the zinc-distal site of the inhibitor forms hydrogen bonds with the protein, while the water at the proximal side lies in a network of well-defined structural water.

Overall, the central scaffold and the distal pyridyl group of **1** form intricate interactions with the specificity loop of MMP-13, which defines the shape and size of the S1′* pocket. Correspondingly, the complex structures of MMP-13cd with pyrimidine dicarboxamides (**1**, **3**, **4**) exhibit continuous and well-defined electron density for this loop and the inhibitors. A comparison with the two publicly available X-ray structures (Protein Data Bank [PDB] entries 830C and 456C [16]), 16 further complex structures with nonpyrimidine dicarboxamide inhibitors (C.K.E., unpublished data), and two NMR structures (PDB entries 1FM1 and 1EUB [25]) suggests

Table 1. Crystallographic Data

	Compound 1	Compound 3	Compound 4
Data processing			
Resolution (Å) (last shell)	1.85 (1.90–1.85)	1.70 (1.80–1.70)	1.80 (1.90–1.80)
Space group	C2	C2	C2
Asymmetric unit	two monomers	two monomers	two monomers
Cell constants a, b, c (Å); β (°)	134.5, 36.5, 95.6; 130.5	134.4, 36.5, 95.3; 130.5	134.0, 36.5, 95.1; 130.4
Total reflections	107,204	133,888	108,348
Unique reflections	30,251	38,478	30,796
R_{sym} (%)[a]	3.5 (7.1)	5.2 (10.3)	5.2 (10.1)
Completeness (%)	98.4 (90.0)	97.8 (90.5)	93.0 (60.9)
Mean I/σ	22.4 (10.7)	14.7 (8.2)	17.7 (8.6)
Refinement			
R_{cryst} (%)[b]	16.6	17.2	16.8
R_{free} (%)[c]	20.2	20.0	20.3
Rmsd bonds (Å)	0.0046	0.0043	0.0044
Rmsd angles (°)	1.19	1.18	1.18
No. of protein atoms	2,675	2,675	2,675
No. of solvent atoms	489	445	473
No. of ligand atoms	2 × 26	2 × 28	2 × 30

[a] $R_{sym}(I) = \Sigma_{hkl}\Sigma_i|I_{hkl,i} - \langle I_{hkl}\rangle|/\Sigma_{hkl}\Sigma_i|I_{hkl,i}| \times 100$, for all independent reflections and i observations of a given reflection. $\langle I_{hkl}\rangle$ is the mean intensity of the i observations.

[b] $R_{cryst} = \Sigma||F_o| - |F_c||/\Sigma|F_o| \times 100$, where F_o and F_c are observed and calculated structure factors, respectively.

[c] R_{free} is the crossvalidation R factor computed for a test set of reflections (5% of the total), which are omitted in the refinement process.

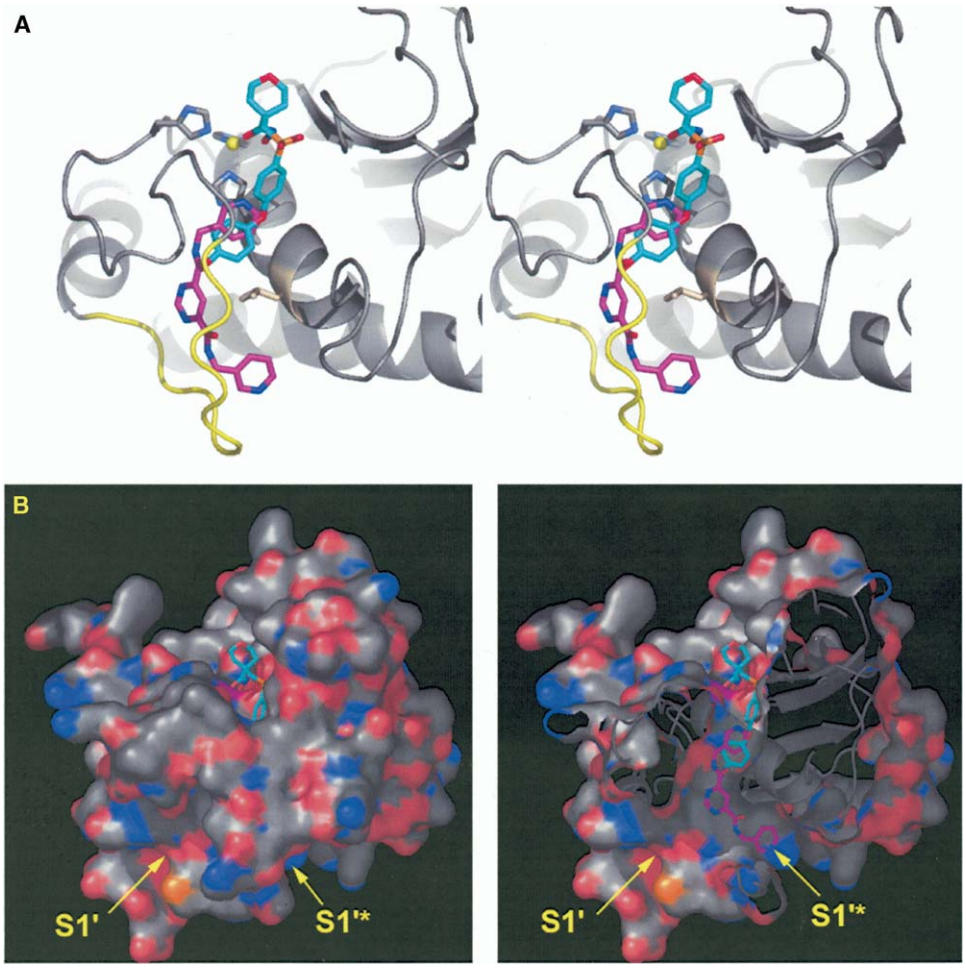

Figure 2. Binding Mode of Pyrimidine Dicarboxamides Exemplified by Inhibitor 1

(A) Stereo graphic of MMP-13cd (gray ribbon representation). The catalytic zinc (yellow sphere), the specificity loop (yellow ribbon), inhibitor 1 (magenta), and Leu218 (gold) are highlighted. Inhibitor 1 is binding without contacting the catalytic zinc, deeply within the S1′ pocket, where it packs onto Leu218 and extends into the S1′* pocket. For comparison, the zinc-chelating hydroxamate MMP-inhibitor RS-130830 (light blue) was superimposed from PDB entry 830c [16].

(B) Molecular surface of MMP-13cd in a similar orientation. The surface is color coded with carbon atoms shown in gray, oxygen, red; nitrogen, blue; and sulfur, yellow. At left is shown the molecular surface with the hydroxamate inhibitor RS-130830 visible at the active site. On the opposite side of the molecule, the back entrances of the S1′ pocket and the S1′* pocket are depicted with arrows. At right is shown the cut molecular surface. The cutting plane opens the view onto S1′ and S1′* with 1 and superimposed RS-130830.

that the specificity loop of MMP-13 exhibits significant flexibility when it is not in contact with inhibitors like 1 [16, 25]. Inhibitor 1, therefore, appears to select a particular specificity loop conformation from a conformational ensemble in apo MMP-13.

Selectivity against Other MMPs

In order to analyze the structural determinants for the MMP-13 selectivity of pyrimidine dicarboxamide inhibitors, the structures of 11 MMP catalytic domains with published three-dimensional structure (MMP-1, -2, -3, -7, -8, -9, -10, -11, -12, -14, and -16 [16, 17, 26–40]) were superimposed with the complex structure of MMP-13 and 1 (Figures 4 and 5). Visual inspection of the superposition and the inhibitor binding pocket suggests the nature of the residue in position 218 (MMP-13 numbering) and the sequence and conformation of the MMP-specificity loop as determinants for the MMP selectivity of 1.

The X-ray structures show that the packing interaction of 1 with Leu218 is critical for the formation of the inhibitor complex (Figure 3A). Most MMPs carry a leucine residue in the position equivalent to Leu218 in MMP-13 as well. However, MMP -1, -7, and -11 carry bulkier residues in position 218 (Figure 4), which would prohibit complex formation due to steric hindrance.

The particular conformation that the specificity loop of MMP-13 assumes in the complex with 1 is critical for inhibitor binding, since it (1) determines the shape and size of the S1′* pocket, which accommodates the distal arm of 1 (Figure 2B), and (2) determines the exact geometry of polar interactions between the specificity loop and the inhibitor (Figure 3). To investigate the role of the specificity loop conformation for MMP selectivity

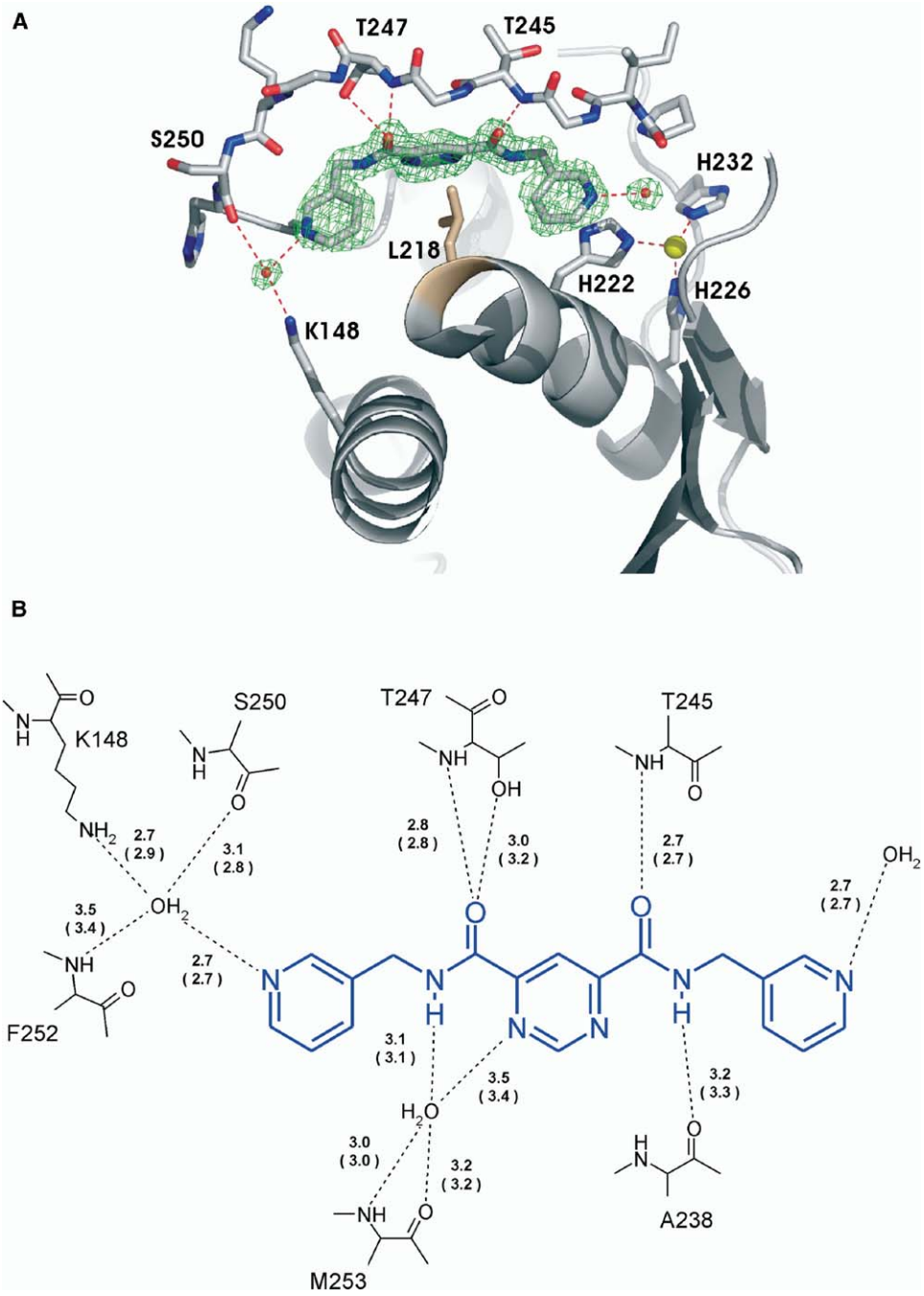

Figure 3. Protein/Inhibitor Interactions

(A) Ribbon representation of MMP-13cd (gray). The inhibitor and several residues are highlighted in stick representation. The side chains of Tyr244 and Tyr246 have been omitted for clarity. Polar interactions are depicted as dashed lines. The 2Fo-Fc electron density is contoured at 2 σ and shown in green. Two structural water molecules are shown in red.

(B) Sketch of polar interactions between **1** and the catalytic domain of MMP-13. Distances are indicated for the two monomers in the asymmetric unit (chain B in parentheses)

of **1**, we inspected the superposition of MMP-13 with the 11 MMP catalytic domains of known three-dimensional structure. As observed for MMP-13, other MMPs also exhibit at least some flexibility in the specificity loop region. Accordingly, 6 of 110 crystallographically independent MMP chains in the PDB exhibit disorder (discontinuous coordinate sets) for the specificity loop. However, it is interesting to observe that for the remaining 104 chains with continuous coordinate sets none of the observed specificity loop conformations is compatible with the steric and geometric requirements for binding of **1**, as exemplified in Figure 5. While we cannot exclude that other MMPs can assume currently unobserved conformations, our biochemical data suggest

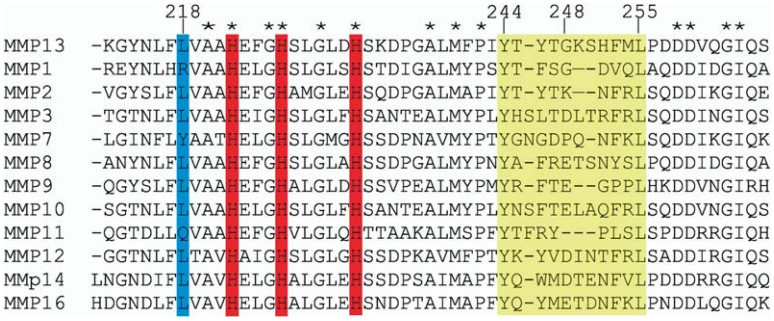

Figure 4. Structure-Based Sequence Alignment of MMPs with Known Three-Dimensional Structure

The region shown corresponds to residues 212–265 of MMP-13 and contains Leu218 (cyan), the catalytic histidines (red), and the specificity loop (residues 244–255, yellow) with Gly248.

that the conformational space of the MMP-13 specificity loop is not accessible for other MMPs. Conformational restrictions appear obvious for those MMPs with specificity loops shorter than that of MMP-13 (Figure 5A), whereas conformational restrictions for MMPs with similar or longer specificity loops must be based on the loops' sequence. In complex with pyrimidine dicarboxamide inhibitors, Gly248 in the specificity loop of MMP-13 assumes a main-chain conformation, which is energetically disfavored for nonglycine residues. We propose that conformational flexibility in this position is crucial for the hydrogen bonding geometry between **1** and the neighboring residues Thr247 and Thr245 (Figure 3). Accordingly, those MMPs that carry a nonglycine residue in an equivalent position may not be able to assume a specificity loop conformation compatible with the binding of **1** (Figure 4).

Overall, this analysis supports the observed selectivity against MMP -1, -2, -3, -7, -8, -9, -10, -12 -14, and -16 (no detectable affinity with detection cutoff at 100 μM) and strongly suggests similar selectivity against MMP-11 (glutamine in position 218).

Inhibitor Design

For the design of improved analogs of **1** (IC_{50} = 6.6 μM), we analyzed molecular properties of the binding pocket. To start with, we considered the central pyrimidine dicarboxamide moiety as a key anchoring point and kept it invariant. From a synthetic chemistry point of view, the scaffold is amenable to parallel synthesis by coupling the pyrimidine dicarboxamide core to amine building blocks. Instead of synthesizing large compound libraries, we decided to use the crystal structures to probe interactions with a limited number of amines. Our design strategy included three steps, which are exemplified by inhibitors **2**–**4**: (1) the replacement of the relatively polar pyridyl substitutions with less polar residues, (2) probing potential entropy gains from displacement of structural water around the pyridyl nitrogens of **1**, and (3) optimizing van der Waals interactions with side chains in the vicinity of the inhibitor.

Closer inspection of the inhibitor interactions with MMP-13 reveals a π-stacking interaction between the proximal pyridine of **1** and His222, while the distal pyridine of **1** is involved in interactions with a cluster of lipophilic side chains from Phe217, Leu218, Tyr246, and Phe252. Together, these observations suggested probing nonpolar aromatic replacements of the pyridyl of **1**, as exemplified by the benzyl analog **2**, which exhibited an activity increase of 1.5 orders of magnitude (IC_{50} = 400 nM).

As a second step, we probed substitutions at the benzyl group in order to displace the structural water and increase hydrophobic interactions at the outer rings of the inhibitor. Inhibitor **3** (IC_{50} = 72 nM) has a methyl group pointing in the direction of the structural water seen in our original structure (Figure 3). A comparison of the X-ray structures of MMP-13cd in complex with **1** and **3** provided a detailed view of the water structure around the inhibitor binding site. At the proximal site, the replacement of the pyridyl substitution in **1** by a methyl-benzyl group in **3** leads to a net displacement of two structural water molecules from the protein inhibitor complex (Figure 6). At the distal site, the same substitution results in a shift of one structural water without altering the net sum of structural waters around the inhibitor.

As a third step, the addition of a fluoro group in inhibitor **4** led to an improved IC_{50} of 8 nM, which likely results from improved interactions with residues Leu185, Val219, and Asp223 at the proximal site and Lys140, Asn215, and Phe217 at the distal site. The complex structure with **4** shows that the net sum of structural water around the inhibitor is unchanged with respect to compound **3** (Figure 6).

Significance

Matrix metalloproteinases (MMPs) are a family of zinc endopeptidases involved in the homeostasis of the extracellular matrix. Abnormal activity of these enzymes has been related to a variety of pathologic processes, involving metastasis, angiogenesis, cardiovascular disease, osteoarthritis, and rheumathoid arthritis [3]. The development of potent subclass-selective inhibitors of these enzymes has been challenging, and most described inhibitors rely on a small number of zinc binding motifs [5]. The X-ray structures reported in this paper reveal a class of highly selective inhibitors of MMP-13 that do not interact with the catalytic zinc but bind deeply in the S1′ pocket of MMP-13, from which they protrude into a side pocket (S1′*) that has not been observed in other MMPs.

A structural alignment with the catalytic domains of 11 MMPs suggests the nature of the residues in position 218 and 248 as well as the sequence and conformation of the specificity loop (residues 244–255 in

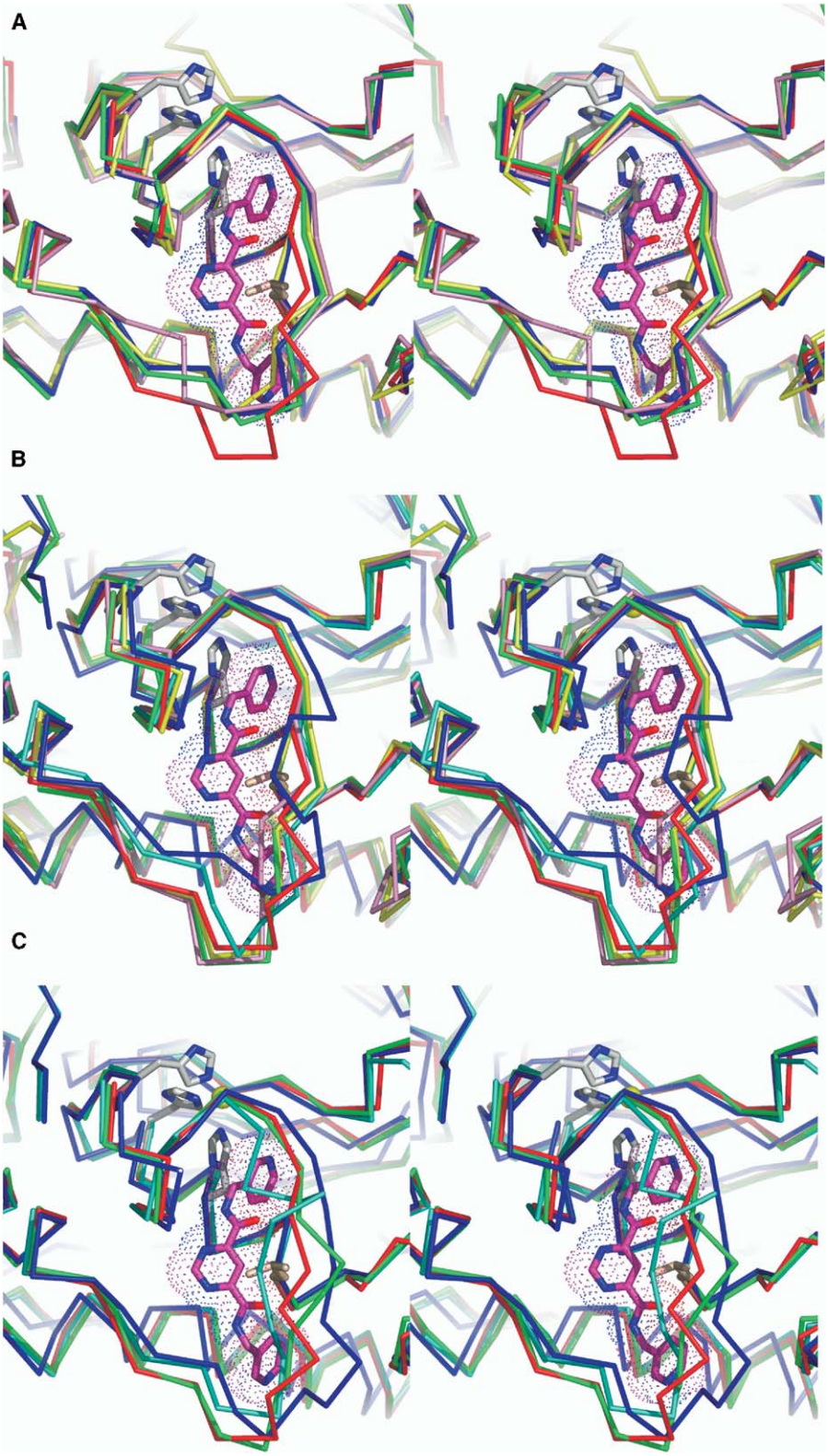

Figure 5. Comparison of MMP Structures

The complex structure with 1 is depicted invariantly with the protein Cα-trace (red), inhibitor 1 (magenta), and the corresponding van der Waals surface of the inhibitor (dots). The specificity loop in MMP-13 has a length of 11 residues.

(A) Superposition of MMP-13 with MMPs with shorter specificity loops: MMP-1 (blue, nine residues), MMP-2 (green, nine residues), MMP-9 (pink, nine residues), and MMP-11 (yellow, nine residues).

(B) Superposition of MMPs with specificity loops of identical length, as in MMP-13: MMP-7 (blue), MMP-8 (green), MMP-12 (cyan), MMP-14 (yellow), and MMP-16 (pink).

(C) Superposition with MMPs with longer specificity loops: MMP-10 (green, 12 residues) and two distinct loop conformations of MMP-3 (blue and cyan, 12 residues).

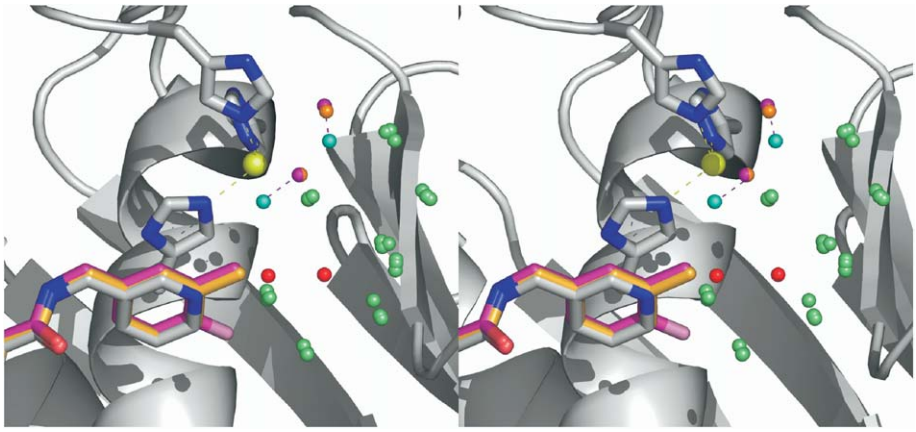

Figure 6. Water Networks at the Proximal Site

A stereo graphic of MMP-13 (gray ribbon diagram) is shown with the active site histidines (sticks) and the catalytic zinc (yellow sphere). Superimposed are inhibitors **1** (gray), **3** (orange), and **4** (magenta) and the three corresponding water networks at the proximal site. Water molecules that are found in almost identical positions in all three structures are colored in bright green. Otherwise, waters are colored according to the inhibitor complex they belong to: complex with **1**, red and cyan; **3**, orange; and **4**, magenta. The two water molecules from the complex structure with **1** shown in red are displaced in the complexes with **3** and **4**. The two water molecules shown in cyan are shifted upon binding of **3** or **4** (magenta dashed lines).

MMP-13) as structural determinants for the high MMP selectivity of these molecules. Rational design of inhibitors with low nanomolar affinity involved improvement of hydrophobic interactions and the replacement of structural water molecules.

Experimental Procedures

Assays

Pro MMP-13 (G25-C471) was prepared according to the procedure of Okada et al. [41] (Invitek, Berlin, Germany). Activation of the enzyme using 1 mM APMA (4-aminophenymercuric acetate) and subsequent assay of proteolytic activity using a quenched fluorogenic substrate were performed as described by Knight et al. [42]. Each well contained 10 µl enzyme (in 0.1 mol/l Tris/HCl [pH 7.5], 0.1 mol/l NaCl, 0.01 mmol/l $CaCl_2$, 0.015% Brij 35) and 10 µl inhibitor in 3% DMSO. After preincubation for 15 min at 22°C, the reaction was started by addition of 10 µl substrate (75 µmol/l in 0.75% DMSO). Activity measurements for the other MMPs were performed according to the procedure described in Matter et al. [43]. Substrates were (6-(7-nitrobenzyl [1, 2, 5] oxadiazol-4-ylamino)-hexanoyl-arg-pro-lys-pro-leu-ala-nva-trp-lys-(7dimethylaminocoumarin-4-yl)-NH_2 for MMP-10 and (7-methoxycoumarin-4-yl) acetyl-pro-leu-gly-leu-3-(2′,4′-dinitrophenyl)-L-2,3-diaminopropionyl-ala-arg-NH_2 for all other MMPs. The substrates were purchased from Bachem, Heidelberg, Germany. The initial velocity of each enzymatic reaction was determined without inhibitor (= 100%) and with at least five different inhibitor concentrations. Each assay was run in triplicate, and IC_{50} values were calculated based on a four-parameter model [44]. Bioavailability in rats was determined according to the procedure described by Matter et al. [45].

Chemistry

The procedure for preparing compounds **1–4** was as follows: pyrimidine-4,6-dicarboxylic acid (200 mg, 1.2 mmol) was added to $SOCl_2$ (0.3 ml, 4.1 mmol), and the mixture was stirred at 85°C for 2 hr. The resulting mixture was cooled to room temperature and diluted with CH_2Cl_2 (2 ml). The mixture was further cooled to 0°C, triethylamine (0.33 ml, 2.4 mmol) and the appropriate amines (5.4 mmol) were added, and the mixture was stirred for 15 min. The reaction mixture was diluted with CH_2Cl_2 (10 ml) and water (10 ml). The organic layer was washed with brine and dried over $MgSO_4$. Removal of the solvent and crystallization from ethyl acetate/heptene (3:1) gave the title compounds.

Pyrimidine-4,6-Dicarboxylic Acid Bis-[(Pyridin-3-YL-Methyl)-Amide] 1

^{1}H NMR (400 MHz, DMSO-d_6)δ 9.80 (m, 2H), 9.45 (s, 1H), 8.58 (m, 2H), 8.45 (m, 3H), 7.75 (m, 2H), 7.35 (m, 2H), 4.55 (m, 4H); MS (ESI) m/z 348.00 (M^+).

Pyrimidine-4,6-Dicarboxylic Acid Bis-Benzylamide 2

^{1}H NMR (400 MHz, DMSO-d_6)δ 9.70 (m, 2H), 9.45 (s, 1H), 8.48 (s, 1H), 7.32 (m, 8H), 7.25 (m, 2H), 4.52 (m, 4H); MS (ESI) m/z 346.14 (M^+).

Pyrimidine-4,6-Dicarboxylic Acid Bis-(3-Methyl-Benzylamide) 3

^{1}H NMR (400 MHz, DMSO-d_6)δ 9.45 (s, 1H), 8.45 (s, 1H), 7.20 (m, 2H), 7.12 (m, 4H), 7.05 (m, 2H), 4.48 (m, 4H), 2.30 (s, 6H); MS (ESI) m/z 375.13 (M^+).

Pyrimidine-4,6-Dicarboxylic Acid Bis-(4-Fluoro-3-Methyl-Benzylamide) 4

^{1}H NMR (400 MHz, DMSO-d_6)δ 9.65 (m, 2H), 9.42 (s, 1H), 8.55 (s, 1H), 7.22 (m, 2H), 7.15 (m, 2H), 7.08 (m, 2H), 4.50 (m, 4H), 2.40 (s, 6H); MS (ESI) m/z 411.25 (M^+).

Crystallography

Activated recombinant human MMP-13 catalytic domain (Tyr104-Asn274) was purchased from Invitek, Berlin, Germany and stored at –80°C in a solution containing 50 mM Tris-HCl (pH 7.5), 150 mM NaCl, 5 mM $CaCl_2$. For crystallization, the enzyme was concentrated to 10 mg/ml, and crystals were grown by mixing equal volumes of protein and reservoir solution consisting of 0.1 M Tris-HCl (pH 8.0), 17% (w/v) PEG4000, and 1 M ammonium formate in the presence of a low-affinity MMP-13 inhibitor [16]. Compounds **1**, **3**, and **4** were dissolved in DMSO, and MMP-13cd crystals were soaked for 1–3 days in the reservoir solution supplemented with 2.5–5 mM inhibitor. The crystals were cryoprotected in the reservoir solution supplemented with 15% (w/v) PEG400 and flash frozen in liquid nitrogen. Data were collected at beamlines id14-1 and id14-2 at the European Synchrotron Radiation Facility (ESRF), Grenoble, France and processed with XDS and XSCALE [46, 47]. Structures were determined by molecular replacement using PDB entry 830C [16] as search model. Molecular replacement, refinement, and model building were preformed with the programs CNX [48] and Quanta [49]. The water structures were generated with a semi-automated procedure using Quanta. Water molecules were included based on positive $F_o - F_c$ difference density at a 3 σ cutoff

level and a 1 σ cutoff in $2F_o - F_c$ electron density maps after subsequent refinement. Structures were analyzed and visualized with CCP4 software [50] and Pymol [51].

Accession Numbers

The coordinates have been deposited in the Protein Data Bank with accession codes 1XUC, 1XUD, and 1XUR.

Acknowledgments

We thank Volker Jeske, Petra Lönze, and Volker Brachvogel for technical assistance and Herman Schreuder and Hans Peter Nestler for constructive comments on the manuscript. The authors are current or former employees of Aventis Pharma Deutschland GmbH, a company of the Sanofi-Aventis Group, which manufactures the chemicals described here.

Received: September 13, 2004
Revised: October 28, 2004
Accepted: November 1, 2004
Published: February 25, 2005

References

1. Stöcker, W., and Bode, W. (1995). Structural features of a superfamily of zinc-endopeptidases: the metzincins. Curr. Opin. Struct. Biol. *5*, 383–390.
2. Stöcker, W., Grams, F., Baumann, U., Reinemer, P., Gomis-Rüth, F.-X., McKay, D.B., and Bode, W. (1995). The metzincins: Topological and sequential relations between the astacins, adamalysins, serralysins, and matrixins (collagenases) define a superfamily of zinc peptidases. Protein Sci. *4*, 823–840.
3. Greenwald, R.A., Zucker, S., and Golub, L.M., eds. (1999). Inhibition of Matrix Metalloproteinases: Therapeutic Applications. (New York: New York Academy of Sciences).
4. Freije, J.M.P., Diez-Itza, I., Balbin, M., Sanchez, L.M., Blasco, R., Tolivia, J., and Lopez-Otin, C. (1994). Molecular cloning and expression of collagenase-3, a novel human matrix metalloproteinase produced by breast carcinomas. J. Biol. Chem. *269*, 16766–16773.
5. Matter, H., and Schudok, M. (2004). Recent advances in the design of matrix metalloproteinase inhibitors. Curr. Opin. Drug Disc. Devel. *7*, 513–535.
6. Wernicke, D., Seyfert, C., Hinzmann, B., and Gromnica, I.E. (1996). Cloning of collagenase 3 from the synovial membrane and its expression in rheumatoid arthritis and osteoarthritis. J. Rheumatol. *23*, 590–595.
7. Aigner, T., Zien, A., Gehrsitz, A., Gebhard, P.M., and McKenna, L. (2001). Anabolic and catabolic gene expression pattern analysis in normal versus osteoarthritic cartilage using complementary DNA-array technology. Arthritis Rheum. *44*, 2777–2789.
8. Shlopov, B.V., Gumanovskaya, M.L., and Hasty, K.A. (2000). Autocrine regulation of collagenase 3 (matrix metallo-proteinase 13) during osteoarthritis. Arthritis Rheum. *43*, 195–205.
9. Kevorkian, L., Young, D.A., Darrah, C., Donell, S.T.,, Shepstone, L., Porter, S.,, Brockbank, S.M.V., Edwards, D.R., Parker, A.E., and Clark, I.M. (2004). Expression profile of metalloproteinases and their inhibitors in cartilage. Arthritis Rheum. *43*, 131–141.
10. Wojtowicz-Praga, S., Torri, J., Johnson, M., Steen, V., Marshall, J., Ness, E., Dickson, R., Sale, M., Rasmussen, H.S., Chiodo, T.A., et al. (1998). Phase I trial of Marimastat, a novel matrix metalloproteinase inhibitor, administered orally to patients with advanced lung cancer. J. Clin. Oncol. *16*, 2150–2156.
11. Michaelides, M.R., and Curtin, M.L. (1999). Recent advances in matrix metalloproteinase inhibitors research. Curr. Pharm. Des. *5*, 787–819.
12. Skotnicki, J.S., DiGrandi, M.J., and Levin, J.I. (2003). Design strategies for the identification of MMP-13 and TACE inhibitors. Curr. Opin. Drug Disc. Devel. *6*, 742–759.
13. Whittaker, M., Floyd, C.D., Brown, P., and Gearing, A.J.H. (1999). Design and Therapeutic Application of Matrix Metalloproteinase Inhibitors. Chem. Rev. *99*, 2735–2776.
14. Skiles, J.W., Gonnella, N.C., and Jeng, A.Y. (2001). The design, structure, and therapeutic application of matrix metalloproteinase inhibitors. Curr. Med. Chem. *8*, 425–474.
15. Chen, J.M., Nelson, F.C., Levin, J.I., Mobilio, D., Moy, F.J., Nilakantan, R., Zask, A., and Powers, R. (2000). Structure-based design of a novel, potent, and selective inhibitor for MMP-13 utilizing NMR spectroscopy and computer-aided molecular design. J. Am. Chem. Soc. *122*, 9648–9654.
16. Lovejoy, B., Welch, A.R., Carr, S., Luong, C., Broka, C., Hendricks, R.T., Campbell, J.A., Walker, K.A.M., Martin, R., Van Wart, H., et al. (1999). Crystal structures of MMP-1 and –13 reveal the structural basis for selectivity of collagenase inhibitors. Nat. Struct. Biol. *6*, 217–221.
17. Stams, T., Spurlino, J.C., Smith, D.L., Wahl, R.C., Ho, T.F., Qoronfleh, M.W., Banks, T.M., and Rubin, B. (1994). Structure of human neutrophil collagenase reveals large S1' specificity pocket. Nat. Struct. Biol. *1*, 119–123.
18. Welch, A.R., Holman, C.M., Huber, M., Brenner, M.C., Browner, M.F., and Van Wart, H.E. (1996). Understanding the P1' specificity of the matrix metalloproteinases: effect of S1' pocket mutations in matrilysin and stromelysin-1. Biochemistry *35*, 10103–10109.
19. Puerta, D.T., Lewis, J.A., and Cohen, S.M. (2004). New beginnings for matrix metalloproteinase inhibitors: Identification of high-affinity zinc-binding groups. J. Am. Chem. Soc. *126*, 8388–8389.
20. Babine, R.E., and Bender, S.L. (1997). Molecular recognition of protein-ligand complexes: applications to drug design. Chem. Rev. *97*, 1359–1472.
21. Schroeder, J., Henke, A., Wenzel, H., Brandstetter, H., Stammler, H.G., Stammler, A., Pfeiffer, W.D., and Tschesche, H. (2001). Structure-based design and synthesis of potent matrix metalloproteinase inhibitors derived from a 6H–1,3,4-thiadiazine scaffold. J. Med. Chem. *44*, 3231–3243.
22. Foley, L.H., Palermo, R., Dunten, P., and Wang, P. (2001). Novel 5,5-disubstituted pyrimidine-2,4,6-triones as selective MMP inhibitors. Bioorg. Med. Chem. Lett. *11*, 969–972.
23. Jacobsen, E.J., Mitchell, M.A., Hendges, S.K., Belonga, K.L., Skaletzky, L.L., Stelzer, L.S., Lindberg, T.J., Fritzen, E.L., Schostarez, H.J., O'Sullivan, T.J., et al. (1999). Synthesis of a series of stromelysin-selective thiadiazole urea matrix metalloproteinase inhibitors. J. Med. Chem. *42*, 1525–1536.
24. Andrianjara, C., Ortwine, D.F., Pavlovsky, A.G., and Roark, W.H. (2002). Matrix Metalloproteinase Inhibitors. WO 02/064080 A2.
25. Zhang, X., Gonnella, N.C., Koehn, J., Pathak, N., Ganu, V., Melton, R., Parker, D., Hu, S.-I., and Nam, K.-Y. (2000). Solution structure of the catalytic domain of human collagenase-3 (MMP-13) complexed to a potent non-peptidic sulfonamide inhibitor: binding comparison with stromelysin-1 and collagenase-1. J. Mol. Biol. *301*, 513–524.
26. Lovejoy, B., Cleasby, A., Hassell, A.M., Longley, K., Luther, M.A., Weigl, D., McGeehan, G., McElroy, A.B., Drewry, D., Lambert, M.H., et al. (1994). Structure of the catalytic domain of the fibroblast collagenase complexed with inhibitor. Science *263*, 375–377.
27. Dhanaraj, V., Williams, M.G., Ye, Q.-Z., Molina, F., Johnson, L.L., Ortwine, D.F., Pavlovsky, A., Rubin, J.R., Skeean, R.W., White, A.D., et al. (1999). X-ray structure of gelatinase a catalytic domain complexed with a hydroxamate inhibitor. Croat. Chem. Acta *72*, 575–591.
28. Morgunova, E., Tuuttila, A., Bergmann, U., and Tryggvason, K. (2002). Structural insight into the complex formation of latent matrix metalloproteinase 2 with tissue inhibitor of metalloproteinase 2. Proc. Natl. Acad. Sci. USA *99*, 7414–7419.
29. Natchus, M.G., Bookland, R.G., Laufersweiler, M.J., Pikul, S., Almstead, N.G., De, B., Janusz, M.J., Hsieh, L.C., Gu, F., Pokross, M.E., et al. (2001). Development of new carboxylic acid-based MMP inhibitors derived from functionalized propargylglycines. J. Med. Chem. *44*, 1060–1071.
30. Becker, J.W., Marcy, A.I., Rokosz, L.L., Axel, M.G., Burbaum, J.J., Fitzgerald, P.M., Cameron, P.M., Esser, C.K., Hagmann,

W.K., Hermes, J.D., et al. (1995). Stromelysin-1: three-dimensional structure of the inhibited catalytic domain and of the C-truncated proenzyme. Protein Sci. *4*, 1966–1976.
31. Browner, M.F., Smith, W.W., and Castelhano, A.L. (1995). Matrilysin-inhibitor complexes: common themes among metalloproteases. Biochemistry *34*, 6602–6610.
32. Gavuzzo, E., Pochetti, G., Mazza, F., Gallina, C., Gorini, B., D'Alessio, S., Pieper, M., Tschesche, H., and Tucker, P.A. (2000). Two crystal structures of human neutrophil collagenase, one complexed with a primed-and the other with an unprimed-side inhibitor: implications for drug design. J. Med. Chem. *43*, 3377–3385.
33. Rowsell, S., Hawtin, P., Minshull, C.A., Jepson, H., Brockbank, S., Barratt, D., Slater, A.M., McPheat, W., Waterson, D., Henney, A., et al. (2002). Crystal structure of MMP-9 in complex with a reverse hydroxamate inhibitor. J. Mol. Biol. *319*, 173–181.
34. Elkins, P.A., Ho, Y.S., Smith, W.W., Janson, C.A., D'Alessio, K.J., McQueney, M.S., Cummings, M.D., and Romanic, A.M. (2002). Structure of the C-terminally truncated human ProMMP-9, a gelatin binding matrix metalloproteinase. Acta Crystallogr. D Biol. Crystallogr. *58*, 1182–1192.
35. Bertini, I., Calderone, V., Fragai, M., Luchinat, C., Mangani, S., and Terni, B. (2004). Crystal structure of the catalytic domain of human matrix metalloproteinase 10. J. Mol. Biol. *336*, 707–716.
36. Gall, A.L., Ruff, M., Kannan, R., Cuniasse, P., Yiotakis, A., Dive, V., Rio, M.C., Basset, P., and Moras, D. (2001). Crystal structure of the Stromelysin-3 (Mmp-11) catalytic domain complexed with a phosphinic inhibitor mimicking the transition-state. J. Mol. Biol. *307*, 577–586.
37. Nar, H., Werle, K., Bauer, M.M.T., Dollinger, H., and Jung, B. (2001). Crystal structure of human macrophage elastase (MMP-12) in complex with a hydroxamic acid inhibitor. J. Mol. Biol. *312*, 743–751.
38. Lang, R., Kocourek, A., Braun, M., Tschesche, H., Huber, R., Bode, W., and Maskos, K. (2001). Substrate specificity determinants of human macrophage elastase (MMP-12) based on the 1.1 Å crystal structure. J. Mol. Biol. *312*, 731–742.
39. Fernandez-Catalan, C., Bode, W., Huber, R., Turk, D., Calvete, J.J., Lichte, A., Tschesche, H., and Maskos, K. (1998). Crystal structure of the complex formed by the membrane type 1-matrix metalloproteinase with the tissue inhibitor of metalloproteinases-2, the soluble progelatinase a receptor. EMBO J. *17*, 5238–5248.
40. Lang, R., Braun, M., Sounni, N.E., Noel, A., Frankenne, F., Foidart, J.-M., Bode, W., and Maskos, K. (2004). Crystal structure of the catalytic domain of Mmp-16/Mt3-Mmp: characterization of Mt-Mmp specific features. J. Mol. Biol. *336*, 213–225.
41. Okada, Y., Morodomi, T., Enghild, J.J., Suzuki, K., Yasui, A., Nakanishi, I., Salvesen, G., and Nagase, H. (1990). Matrix metalloproteinase 2 from human rheumatoid synovial fibroblasts. Purification and activation of the precursor and enzymic properties. Eur. J. Biochem. *194*, 721–730.
42. Knight, C.G., Willenbrock, F., and Murphy, G. (1992). A novel coumarin-labelled peptide for sensitive continious assays of the matrix metalloproteinases. FEBS Lett. *296*, 263–266.
43. Matter, H., Schwab, W., Barbier, D., Billen, G., Haase, B., Neises, B., Schudok, M., Thorwart, W., Schreuder, H., Brachvogel, V., et al. (1999). Quantitative structure-activity relationship of human neutrophil collagenase (MMP-8) inhibitors using comparative molecular field analysis and x-ray structure analysis. J. Med. Chem. *42*, 1908–1920.
44. Kuzmic, P., Hill, C., and Janc, J.W. (2004). Practical robust fit of enzyme inhibition data. Methods Enzymol. *383*, 366–381.
45. Matter, H., Schudok, M., Schwab, W., Thorwart, W., Barbier, D., Billen, G., Haase, B., Neises, B., Weithmann, K.U., and Wollmann, K. (2002). Tetrahydroisoquinoline-3-carboxylate based matrix-metalloproteinase inhibitors: Design, synthesis and structure-activity relationship. Bioorg. Med. Chem. *10*, 3529–3544.
46. Kabsch, W. (1988). Automatic indexing of rotation diffraction patterns. J. Appl. Crystallogr. *21*, 67–71.
47. Kabsch, W. (1993). Automatic processing of rotation diffraction data from crystals of initially unknown symmetry and cell constants. J. Appl. Crystallogr. *26*, 795–800.
48. Brünger, A.T., Adams, P.D., Clore, G.M., DeLano, W.L., Gros, P., Grosse-Kunstleve, R.W., Jiang, J.S., Kuszewski, J., Nilges, M., Pannu, N.S., et al. (1998). Crystallography & NMR system: A new software suite for macromolecular structure determination. Acta Crystallogr. D Biol. Crystallogr. *54*, 905–921.
49. Molecular Simulations Inc. (1998). QUANTA (computer program). Molecular Simulations Inc., San Diego, CA.
50. CCP4 (Collaborative Computational Project, Number 4)(1994). The CCP4 suite: programs for protein crystallography. Acta Crystallogr. D Biol. Crystallogr. *50*, 760–763.
51. The PyMOL Molecular Graphics System. DeLano Scientific, San Carlos, CA (http://www.pymol.org).